



CdS/CuInS₂ Quantum Dots Cosensitized Solar Cells Using Functionalized Polyurethane Gel Electrolytes

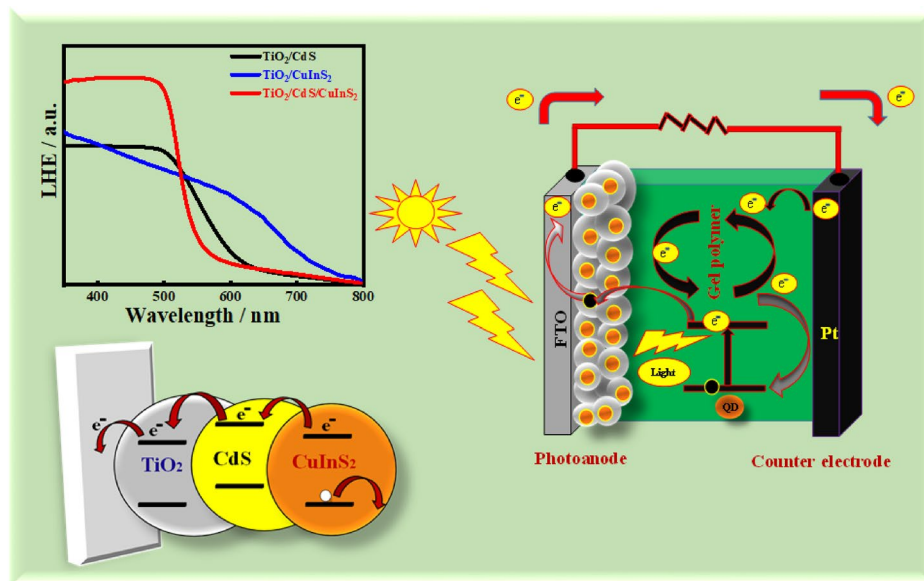
Ravi Prakash¹ · Amita Santra¹ · Sparsh Yaduka¹ · Pralay Maiti¹

Received: 26 December 2023 / Accepted: 29 July 2024
© Indian National Academy of Engineering 2024

Abstract

Functionalized thermoplast polyurethane has been synthesised and further developed as polymer gel electrolyte for quantum dots sensitized solar cells. ¹H NMR, FTIR, and UV–vis spectroscopic technique are used to confirm the functionalization. The CdS and CuInS₂ quantum dots are used to develop the cosensitized photoanode and subsequently used to fabricate photovoltaic devices. The SILAR cycle were used to developed CdS quantum dots on TiO₂ nano-crystalline semiconductors photoanode followed by CuInS₂ quantum dots deposited through spin coating technique. The cosensitized photoanode (TiO₂/CdS/CuInS₂) has higher light harvesting efficiency as compared to single loaded quantum dots (TiO₂/CdS or TiO₂/CuInS₂ photoanode). The energy levels of the highest occupied molecular orbital, lowest unoccupied molecular orbital, valence band, and conduction band for polymer and quantum dots have been estimated through cyclic voltammetry and optical band gap calculated through UV–vis measurements and consequently match the energy levels to optimise the suitable possible combination of materials for devices fabrication. The TiO₂/CdS/CuInS₂ photoanode with developed polymer gel electrolyte shows high power conversion efficiency ~ 1.05%, which is almost 42% greater than that of photoanode without CuInS₂.

Graphical Abstract



Keywords Cosensitizer · Light harvesting efficiency · Quantum dots · Polyurethane

Extended author information available on the last page of the article

Published online: 20 August 2024

Introduction

Global economic expansion is driving up energy use, which highlights the need for a more sustainable energy infrastructure (Song et al. 2018). Nowadays, fossil fuels account for 85.5% of our basic energy needs, creating 75% greenhouse gas emission and causing climate change and global warming (Energy Institute, 2023). About 31.95% (15.18 Gt CO₂) of the world's greenhouse gas emission come from the production of electricity and heat, making it the large contributor (Watch and Emissions 2023). Therefore, it is crucial to realise a clean, renewable power source. Solar energy is an abundant resource, with most human-inhabited areas receiving between 3 to 7 kW-h/m² of radiation per day (Ritchie et al. 2022). Despite this, it accounts for only ~2% of global electricity production (Ritchie et al. 2022). Photovoltaic cells, which convert solar radiation into electricity, are receiving increasing attention in research in terms of efficiency, stability, and affordability. Solar cell technology can be split up into three generations. The first generation consists of crystalline silicon wafer solar cells—the most commercially available cells, having efficiency of ~16% (Green 2001). These cells have high cost of starting materials, manufacturing, and subsequent installation (Green 2001; Kamat 2008). The second generation of solar cells aims to reduce these costs by employing polycrystalline thin films such as GaAs, CdTe, CIGS compound films and amorphous silicon (Wu et al. 2015). However, despite theoretically being able to cross the Shockley-Queisser (S-Q) Limit of 32% efficiency, which applies to traditional cells, (Shockley and Queisser 1961) they currently suffer from low efficiency (5–10%) making them less commercially viable (Green 2001; Kamat 2008). The third generation seeks to increase performance at feasible production costs through technologies such as quantum dots sensitized solar cell, dye sensitized solar cells, perovskite solar cells and tandem cells, hot-carrier extraction, cells based on multiple exciton generation, thermophotovoltaic conversion, among others (Green 2001; Nozik 2002; Kamat 2008). The introduction of the dye sensitized solar cell (DSSC) by Grätzel and O'Regan in 1991, (O'Regan and Grätzel 1991) led to heightened research efforts into the third generation of solar cells and the field of molecular components for photoreception. In DSSCs, organic dyes serve to generate electron–hole pairs which are extracted through a semiconductor layer. As an alternative to organic dyes, semiconductor nanoparticles called quantum dots (QDs), with their size-dependent properties, have received great attention as photosensitizers. (Kamat 2008) Quantum dots are narrow bandgap, zero-dimensional materials

exhibiting size-quantization enabling the tuneability of their photoelectrochemical behaviour and band gap. (Kamat 2008; Kongkanand et al. 2008) The optical properties of QDs are greatly enhanced with confinement (Schmitt-Rink et al. 1987) and the tuneability of these optical properties is advantageous to carrier extraction. (Ross and Nozik 1982; Nozik 2002) The combination of quantization effects and tuneability facilitates the ability to harvest light across the entire visible spectrum of insolation, pushing the maximum possible efficiency to around 44%, in the ideal case. (Ross and Nozik 1982; Nozik 2002, 2021; Bera et al. 2010) Thus, a photoanode structure similar to DSSCs can be fabricated where the organic dye is replaced by quantum dots, resulting in a cell structure called a quantum dot sensitized solar cell (QDSSC). (Kongkanand et al. 2008; Wurfel et al. 2015) Cd-based metal-chalcogenide quantum dots (e.g. CdSe, CdTe, CdS) are well reported and researched as sensitizers for solar cells due to their suitable band gaps, mobilities and extinction coefficients. (Gerischer and Luebke 1986; Vogel et al. 1990; Kohtani et al. 1993; Liu and Kamat 1993; Robel et al. 2006; Lee et al. 2008; Gao et al. 2009; Lan et al. 2009; Badawi et al. 2013; Yang and Zhong 2016) CuInS₂ and CuInSe₂ quantum dots have been explored as less toxic photosensitizers with positive results, often in a core–shell or cosensitized mode. (Li et al. 2011, 2012; Luo et al. 2013; Santra et al. 2013; Jara et al. 2014; Pan et al. 2014; Du, et al. 2016) Cosensitized systems have been observed to perform better than singly sensitized solar cells owing to their extended spectral response and enhanced charge injection, leading to better short circuit current density (J_{sc}). (Lee and Lo 2009; Sudhagar et al. 2009; Wang et al. 2018) Cosensitized solar cells benefit from the complementary optical properties of two quantum dots, whereby QDs with high molar extinction coefficients but narrow spectral ranges, when combined with QDs of wider spectral response, but lower internal efficiencies, result in a system with a wider spectral response and high extinction coefficient. (Lee and Lo 2009; Sudhagar et al. 2009; Wang et al. 2018) CuInS₂ is a semiconductor that is chalcopyrite and has band gap of 1.53 eV. (Shay and Jack 1975) The optimal value needed for an optical absorber in an effective solar cell is corresponding to this value. This compound's ingredients are safe for using. This ternary compound is thought to be a potential contender for solar cell materials based on these distinguished characteristics. Uenishi et al. fabricated a photovoltaic devices using the CdS/CuInS₂ photoanode to receive the 3.1% PCE using the liquid electrolytes. (Uenishi et al. 1994) Mitchell et al. reported the 7.3% PCE with CdS/CuInS₂ photoanode and liquid electrolytes. (Mitchell et al. 1988) The next component in the functional stack of QDSSCs is the electrolyte, which serves to recharge the sensitizing

agents. (Privalov et al. 2009) The electrolyte is, most commonly, a liquid redox mediator couple: I^-/I_3^- (iodide/triiodide) and S^{2-}/S_n^{2-} (polysulphide). (Boschloo and Hagfeldt 2009; Wu et al. 2015) Liquid electrolytes like the polysulphide and I^-/I_3^- redox couple suffer from the inherent risk of corroding inorganic quantum dots at the photoanode, (Okada et al. 2004; Boschloo and Hagfeldt 2009) and devices utilizing liquid electrolytes suffer from long term stability, difficulty in handling and performance degradation due to the volatility of the electrolytes and leakage tendencies. (Boschloo and Hagfeldt 2009; Wu et al. 2015) Exploration of solid-state and quasi-solid state electrolytes, difficulty in handling aim to alleviate these issues. Solid-state electrolytes are highly thermodynamically stable, but suffer from lower ionic conductivity and imperfect contact with electrode components. (Li et al. 2006; Wu et al. 2008; Wu et al. 2015) Quasi-solid state (gel) electrolytes exhibited better performance as compared to solid-state electrolytes due to improved ionic conductivity and suitable electrochemical properties. (Prakash and Maiti 2020).

We have previously fabricated a photovoltaic devices using a $TiO_2/CuInS_2$ photoanodes and functionalized polymer gel electrolytes (SPU-CNT) that included Au (gold) as a counter electrode, and these devices achieved a power conversion efficiency of 0.81%. (Prakash et al. 2023) In this research articles, we demonstrate that an optimum amount of CdS QDs layer deposition in between TiO_2 and $CuInS_2$ QDs shows a significant effect in terms of power conversion efficiency. The fabricated device includes cosensitized photoanode $TiO_2/CdS/CuInS_2$, functionalized polymer gel electrolyte (SPU), and Pt as counter electrode and these fabricated devices show a better performance as compared to the single loaded QDs such as TiO_2/CdS and $TiO_2/CuInS_2$ photoanode.

Experimental

Materials

Cadmium acetate (Sigma Aldrich), TiO_2 paste (Solarnix), titanium tetrachloride ($TiCl_4$, Strem), sodium sulphide (Himedia), indium acetate (sigma aldrich), copper iodide (sigma aldrich), 1-dodecanethiol (sigma aldrich), sodium hydride (NaH), polytetramethylene glycol (PTMG, Mn = 2900, g/mol), 4,4'-Diphenylmethane diisocyanate (MDI, Sigma Aldrich), Butane-diol (Sigma Aldrich), dibutyltindilaurate (DBTDL), N,N-dimethylacetamide (DMA), ethanol (Himedia), propane sultone (Sigma Aldrich) were used as received.

Synthesis of $CuInS_2$ QDs

$CuInS_2$ QDs were synthesized using a one-pot method in which 0.292 g indium acetate and 0.190 g copper iodide were mixed with 5 mL 1-dodecanethiol in a round-bottom flask and degassed. The mixture was purged with nitrogen gas thrice to create an inert atmosphere. Under vigorous stirring, the temperature of the reaction mixture was raised to 1000 °C until a clear solution was obtained, following which, it was further heated to 200 °C. As the temperature increased, the colour of the reaction mixture changes from yellow to dark red, indicating the nucleation and growth of the $CuInS_2$ nanoparticles. To immediately arrest further growth of the nanoparticles, the temperature was quickly reduced to below 50 °C. The resultant QDs were washed with excess methanol with chloroform multiple times. The washed QDs were dried and redispersed in chloroform for characterization.

Synthesis of Polyurethane

A two-step condensation polymerization process was used to synthesized the MDI-based PU: Initially, an isocyanate-terminated prepolymer was prepared by mixing the monomers, 4,4'-methylene diphenyl diisocyanates (MDI) and poly(tetramethylene glycol) (PTMG), in DMF solvent with constant stirring in inert atmosphere at 70 °C for 3 h. Butane-diol was applied to the prepolymer as a chain extender and a small amount (4–5 drops) of DBTDL catalyst in toluene solution was added with constant stirring at the same temperature in an inert environment. Under continuous stirring, the reaction took place over the course of 24 h. Polyurethane was precipitated by adding the final mixture to deionized water. The precipitate was dried in vacuum oven at 50 °C for 72 h.

Functionalization of Polyurethane

The functionalization of polyurethane take place via previously reported bimolecular nucleophilic substitution reaction. Initially, the polymer was dissolved in DMA solvent at 50 °C followed and then cooled to room temperature. Under inert atmosphere and vigorous stirring for one and a half hours, NaH was added to the mixture at – 5 °C. The temperature of the mixture was then brought up to room temperature, and propane sultone was added. Following this, the mixture was heated to 50 °C for 3 h. To isolate the ionomer and remove unreacted chemicals, the resultant mixture was poured into toluene, causing the ionomer to precipitate. The ionomer (SPU) was washed with ethanol three times.

Preparation Gel Electrolytes

To prepare the gel electrolyte, the functionalized polymer was dissolved in DMF solvent. The mixture was heated to 80 °C under constant stirring until a homogeneous mixture was obtained. Subsequently, it was cooled to 5 °C and kept for 18 h, resulting in the formation of the semi-solid ionomer (SPU) gel.

Characterisation

Spectroscopic Measurements

All spectroscopic measurements were performed under ambient temperature. A JASCO V-650 UV–visible spectrophotometer (spectral range: 200–800 nm, scan rate 2 nm / s), was used to evaluate the UV–vis absorbance spectra of the various synthesised quantum dots and polymer thin films. The FTIR spectra of the QDs and polymers were obtained using an Alpha Bruker Eco-ATR instrument (ZnSe ATR crystal, spectral range: 600–4000 cm^{-1}) by performing 100 scans at a resolution of 4 cm^{-1} . ^1H NMR spectra was estimated through Bruker Biospin 500 MHz instrument. The functionalized polymers' chemical shifts were noted in ppm (δ), utilizing DMSO- d_6 as the solvent.

Thermal Analysis

A Mettler-Toledo thermogravimetric analyzer (TGA) was used to evaluate the thermal stability of both pure and functionalized polyurethanes (PUs) in the 40–600 °C temperature range with a heating rate of 20 °C / min. The heat of fusion and melting temperature of pure and functionalized polymers (PUs) were measured through the differential scanning calorimetry (Mettler 832) instruments. The temperature range employed was between – 40° and 200 °C, with a heating and cooling rate of 10°/min and 5°/min, respectively, under nitrogen atmosphere.

Electrochemical Measurements

Electrochemical Impedance Spectroscopy (EIS)

Four probe AC impedance measurements using multichannel Autolab M204 (potentiostat / galvanostat) with frequency response analyzer (FRA 32) were performed to determine the conductivity of the unmodified and functionalized polymers clipped in between two circular titanium electrodes, each with a surface area of 3.14 cm^2 . The applied frequency range from 0.1 to 10^6 Hz with a scan rate of 1 $\mu\text{A/s}$ was used for measurements. A blank spectrum

(Nyquist plot) was recorded, before measuring the sample to account for the resistance of the wire. The fit and simulation method (Nova software ver. 2.1.4) was used to calculate the resistance of polymer which was then used to calculate the ionic conductivity using the following Eq. (1)

$$\kappa^m (\text{S/cm}) = \frac{L(\text{cm})}{[R(\Omega) \times A(\text{cm}^2)]} \quad (1)$$

where, κ^m is the ionic conductivity of the polymer, L is distance between two electrodes, R is the resistance of polymer, A is the area of polymer. The activation energy was calculated using the following Eq. (2)

$$\sigma = \sigma_0 \exp - \frac{E_a}{RT} \quad (2)$$

where, E_a is the activation energy, R is the gas constant, T is temperature, σ is the ionic conductivity.

Cyclic Voltammetry

To conduct the cyclic voltammetry (CV) analysis of QDs and polymer, a multichannel Autolab (Metrohm M204) was used with three electrode setup: glassy carbon as the working electrode, platinum as a counter electrode and Ag/AgCl as a reference electrode. The highest occupied molecular orbitals (HOMO) and lowest unoccupied molecular orbitals (LUMO) energy levels of polymers and QDs were determined using the CV measurements. The HOMO and LUMO of energy level of QDs and polymer was estimated using ferrocene as the reference materials (– 4.4 eV). (Leonat et al. 2013a)

$$E_{HOMO} = -eV(E_{Ox\text{onset}} + 4.4) \quad (3)$$

$$E_{LUMO} = -eV(E_{red\text{onset}} + 4.4) \quad (4)$$

The finely dispersed sample was prepared through ultrasonication of 2 mg of QDs dissolved in 5 mL N-methyl pyrrolidone solvent for 15 min. Suitable working potentials range was determined by performing a blank run of the CV measurement with NMP as solvent. CV analysis of synthesised samples were carried out at room temperature in the potential range of – 2.5 to +2.5 V, at a scan rate of 20 mV/s.

Fabrication of Solar Cells

Preparation of CdS/CuInS₂ Photoanode

$2 \times 1.5 \text{ cm}^2$ FTO glass sheets were cleaned through the process of bath sonication in soap solution, acetone, and distilled water, with each step lasting for 10 min. The

doctor-blade method was employed to deposit a thin film (0.20 cm^2) of TiO_2 paste (Solaronix) on the FTO glass. It was then heated at $75 \text{ }^\circ\text{C}$ for 30 min to eliminate low-boiling organic solvents. Subsequently, annealing was carried out for 30 min at $450 \text{ }^\circ\text{C}$, producing a transparent TiO_2 thin film on the FTO glass. Deposition of CdS quantum dots on TiO_2 was done through successive ionic layer adsorption and reaction (SILAR) method. Each SILAR cycle was involved in four steps: the TiO_2 -coated FTO glass was sequentially immersed in continuously agitated solutions of (1) 1 M cadmium acetate solution for 1 min, (2) washed with methanol for 1 min, (3) sodium sulfide solution for 1 min, and (4) methanol for 1 min at room temperature. This process was repeated for a varying number of cycles, producing samples ranging from yellow to orange. Via ultrasonication for 15 min, CuInS_2 QDs were dispersed in isopropanol. A spin coater (SpinNXG-PI) was used to deposit the CuInS_2 QDs onto the TiO_2/CdS film at 1500 rpm for 15 min, forming a uniform $\text{TiO}_2/\text{CdS}/\text{CuInS}_2$ film. During the photoanode preparation, each QD layer was dried for 30 min at $75 \text{ }^\circ\text{C}$ for solvent removal, ensuring optimal film formation. Until they were utilized in cell fabrication, prepared photoanodes were stored at room temperature in the dark, under vacuum.

Preparation of Counter Electrode

The counter electrode utilized was a Pt thin film with an equivalent 0.20 cm^2 , active area deposited on FTO glass using the doctor-blade method. To eliminate low-boiling organic binders, it underwent heating for 30 min at $80 \text{ }^\circ\text{C}$. Subsequent annealing for 30 min at $450 \text{ }^\circ\text{C}$ ensured uniform formation of a Pt film. For the fabrication of QDSSCs, an adequate amount of gel electrolyte (SPU) was sandwiched between the counter electrode and photoanode, while ensuring the gel was evenly spread across the active areas. To ensure good contact alongside preventing the penetration of the gel electrolyte, a non-conductive thermoplastic spacer (Solaronix Meltonix 1170-25, 0.25 mm thick), was placed between the active and counter-electrodes.

Solar Cell Measurement

The current–potential (I–V) characteristics of the QDSSCs were determined through a multichannel Autolab M204 potentiostat/galvanostat in conjunction with an LED Driver capable of a 700 mA output. The Autolab LED Driver utilized a highly focused light source, and the output of the LED light source was regulated through programmable software connected to the optical bench. The efficiency of QDSSCs was assessed based on three key parameters: open-circuit voltage (V_{oc}), short-circuit current density (J_{sc}) and

fill factor (FF). The power conversion efficiency (η) of the QDSSCs is dependent on these parameters. The calculations for these parameters were carried out using the following equations:

$$FF = \frac{J_{max}}{J_{sc}} \times \frac{V_{max}}{V_{oc}} \text{ or } FF = \frac{P_{max}}{J_{sc} \times V_{oc}} \quad (5)$$

$$\eta(\%) = \frac{P_{max}}{P_{in}} \times 100 \text{ or } \eta(\%) = \frac{J_{sc} \times V_{oc} \times FF}{P_{in}} \times 100 \quad (6)$$

Results and Discussion

Figure 1a represents the synthesis and functionalization of the polyurethane (PU) polymer to be used as hole transporting agent. The synthesis and functionalization of PU polymer was carried out by previously reported method. (Prakash and Maiti 2020) First, prepolymer is formed through the reaction of MDI and PTMG followed by long chain PU is synthesized using butanediol as chain extender in the presence of catalyst (DBTDL).

The sulfonate group has been attached in the main chain of PU using the propane sultone via nucleophilic substitution reaction, hence, introducing the ionic groups in hydrophobic PU chains. The FTIR and ^1H NMR spectroscopy have verified for the attachment of sulfonate groups. A new sharp peak at chemical shift $\delta \sim 8.44 \text{ ppm}$ appears in functionalized PU (SPU) is due to sulfonate proton, while this peak is absent in pure PU. The propane sultone groups present in the functionalized PU results in the appearance of three additional new peaks at chemical shift $\delta \sim 4.47$, 1.72 , and 1.6 ppm which in turn confirms the attachment of the sulfonate moiety ($\text{CH}_2\text{-CH}_2\text{-CH}_2\text{-SO}_3\text{H}$) at the main chain of PU polymer. The FTIR spectroscopic measurements of pure PU and SPU polymer are represented in Fig. 1c. Pure PU has a peak at 3308 cm^{-1} , attributed to the hydrogen bonded $>\text{NH}$ group found in its hard segment, while a broad signal appears at 3382 cm^{-1} in functionalized PU. A strong intense peak has appeared at 1171 cm^{-1} due to the $\text{S}=\text{O}$ linkage which is absent in pure PU, which further confirms the attachments of sulfonate group at the main polymeric chains of PU. The UV–vis absorption spectra of functionalized and pure PU are shown in Fig. 1d. Pure PU shows a peak at 287 nm due to $n \rightarrow \pi^*$ transition, while 335 nm ($n \rightarrow \pi^*$) broad peak is noticed in the functionalized PU. (Leonat et al. 2013b) The functionalized PU have higher light harvesting capacity as compared to the pure PU, thereby better suitable for solar application. (Prakash and Maiti 2020) Pure PU has a melting temperature of $20.4 \text{ }^\circ\text{C}$, but SPU has a significantly higher melting temperature of about $50.8 \text{ }^\circ\text{C}$ (Fig. 1e), presumably due to the interaction

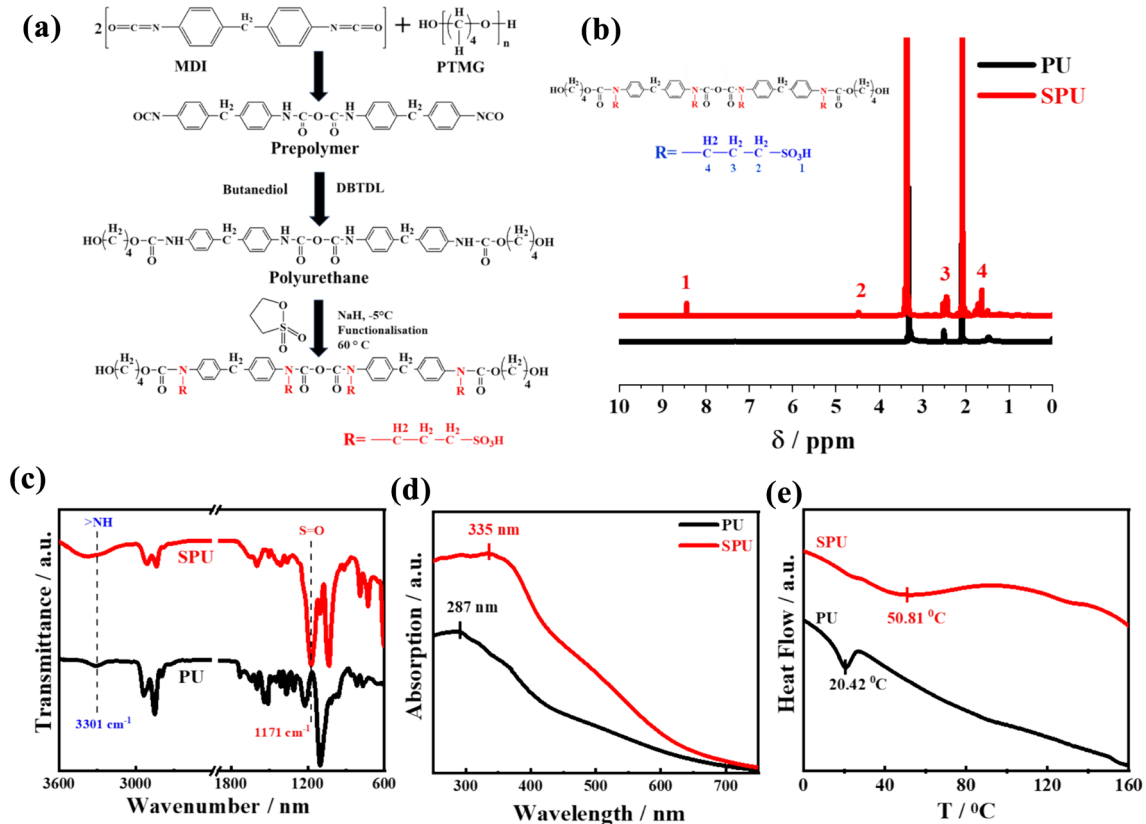


Fig. 1 **a** Reaction scheme for the synthesis of PU and its subsequent functionalization; **b** ^1H NMR spectra of pure and functionalized PU as indicated; **c** FTIR spectra of pure and functionalized PU; **d** UV–

Vis absorption spectra of PU and SPU showing the characteristic peak position; and **e** DSC traces of PU and SPU indicating the melting temperature of respective specimens

between the polar $>\text{NH}$ group in the hard segment of PU and the ionic sulfonate moiety. Figure 2a shows the FTIR spectra of CdS and CuInS_2 QDs. CdS QDs exhibit two significant stretching vibration at 704 and 1610 cm^{-1} , responsible for Cd-S bonds, (Gu et al. 2019) which confirms the growth of CdS quantum dots on the TiO_2 surface. Similarly, the DDT capped CuInS_2 QDs shows three peaks at 2954 , 2919 , and 2850 cm^{-1} , assigned to $-\text{CH}_3$ asymmetric stretching, $-\text{CH}_2$ asymmetric and $-\text{CH}_2$ symmetric stretching vibration, respectively. (Xia et al. 2014) The bands appear at 716 and 1259 cm^{-1} are corresponding to C-S stretching vibration and $-\text{CH}_2\text{S}$ wagging vibration. (Xia et al. 2014) Hence, the use of DDT as capping agent is confirmed and DDT capped CuInS_2 QDs has been formed. The UV–vis absorption spectra of the CdS and CuInS_2 QDs are represented in Fig. 2b. The characteristics absorption peaks for CdS and CuInS_2 QDs are 481 and 573 nm , respectively, (Liu et al. 2012; Gu et al. 2019) which confirm the formation of CdS and CuInS_2 QDs. The optical band gap of CdS and CuInS_2 QDs are calculated using the Tauc's plots which are shown in Fig. 2c, showing the value of 2.18 and 1.85 eV , respectively. Transmission electron microscopy (TEM) bright-field images are used to estimate the particle size of CuInS_2 QDs

and the average particle size $\sim 2\text{ nm}$ is observed. This is to mention that CdS is deposited onto TiO_2 surface through SILAR method.

Electrochemical Analyses

Charge Transport Properties

The performance of the photovoltaic device depends on the resistance of the electrolytes. Usually polymer gel electrolytes with low resistance and strong ionic conductivity make it easier for the hole transportation in the devices operational mode. The ionic conductivity of the polymer is determined by using electrochemical impedance spectrometry (EIS) measurements technique. Utilising the fit and stimulation approach, the polarising resistance of the polymer is determined from the Nyquist plots and are shown in Fig. 3a. The resistance of pure PU is found to be $5.54 \times 10^8\ \Omega$ and after the attachments of sulfonate moiety on the polymeric chains (SPU), reduces the resistance ($4.15 \times 10^2\ \Omega$) resulting significant increase in the conductivity of the functionalized polymer (SPU). The electronic conductivity of SPU polymer

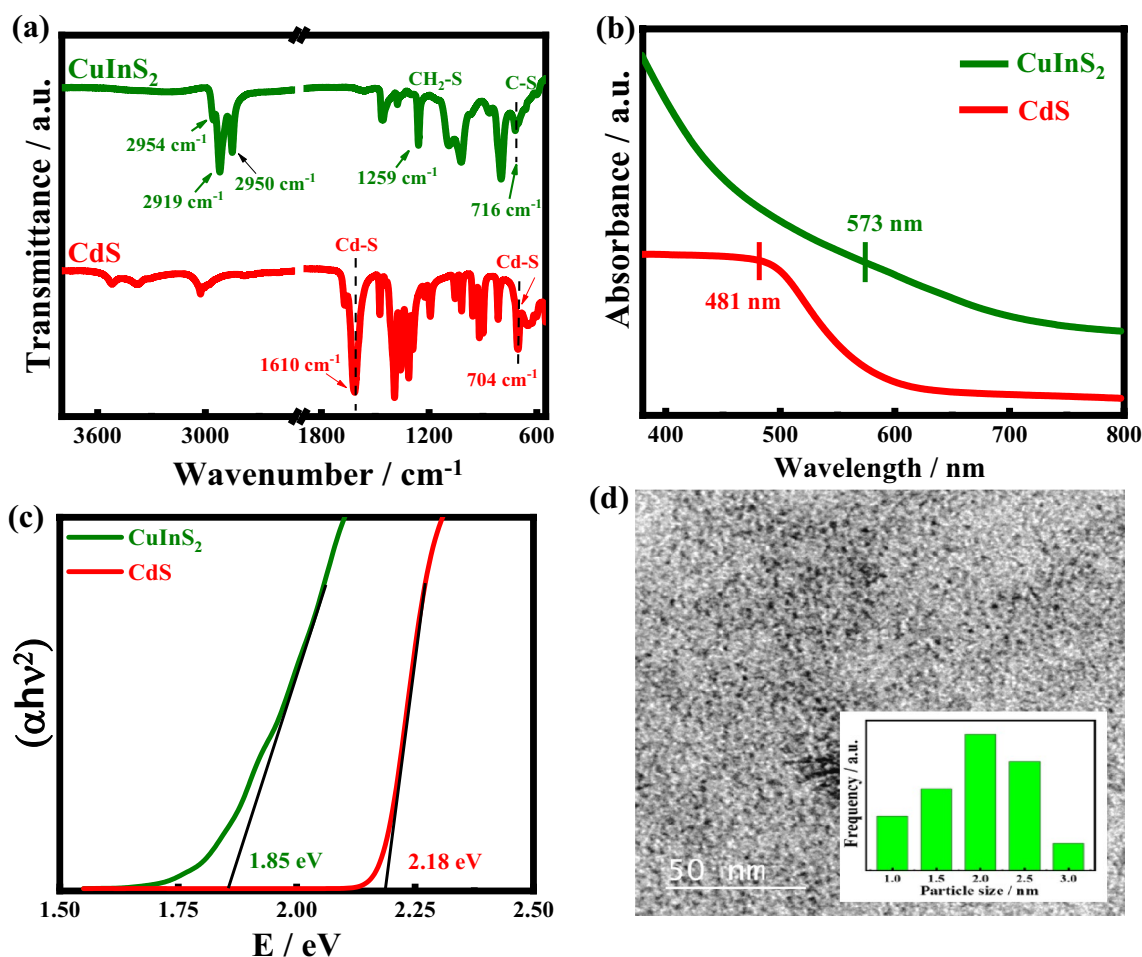


Fig. 2 **a** FTIR spectrum of CdS and CuInS₂ QDs indicating the characteristics peaks; **b** UV–Vis absorption spectra of the CdS and CuInS₂ QDs indicating the absorption peaks; **c** optical band gap of

CdS and CuInS₂ QDs as measured through UV–Vis spectra; **d** Bright field TEM image of the CuInS₂ and inset diagram show the distribution of particles

is found to 6.51×10^{-3} S / cm, similar with the literature report. (Prakash and Maiti 2020) Hence, the synthesised SPU polymer becomes more suitable for the photovoltaic device application.

The EIS measurements are carried out at various temperature and the Arrhenius plots of the polymers (pure PU and SPU) fitted using the Eq. (2) are shown in Fig. 3b showing considerable higher conductivity level of functionalized PU as compared to pristine PU. The Bode plots of the QDSSCs with pure PU and SPU gel electrolytes are shown in Fig. 3c. The peak position in the spectrum curve can be used to determine the electron lifetime according to following Eq. (7). (Tian et al. 2014)

$$\tau = \frac{1}{2\pi f_{\min}} \quad (7)$$

where, τ is electron life time, f_{\min} is the peak frequency corresponding to the charge transfer process at the

photoanode / electrolytes interface. The electron lives longer in the QDSSCs based on SPU gel (1.274×10^{-2} s) as compared to pure PU gel electrolytes (7.977×10^{-7} s). The higher electron life time can be attributed to the reduced recombination process, resulting in the enhance of electron transfer by increasing the electron density and improving power conversion efficiency of the fabricated devices. (Yang et al. 2016).

Energy Profile Diagram

Cyclic voltammetry measurements are useful technique for estimating the produced current when applying voltage at certain scan rate analysing the electrochemical behaviour of materials at electrode–electrolyte interface. The polymer chain becomes a negatively charged species during a redox reaction through a reduction process, and behave a positively charged species during an oxidation reaction. In CV measurements, two distinct peaks

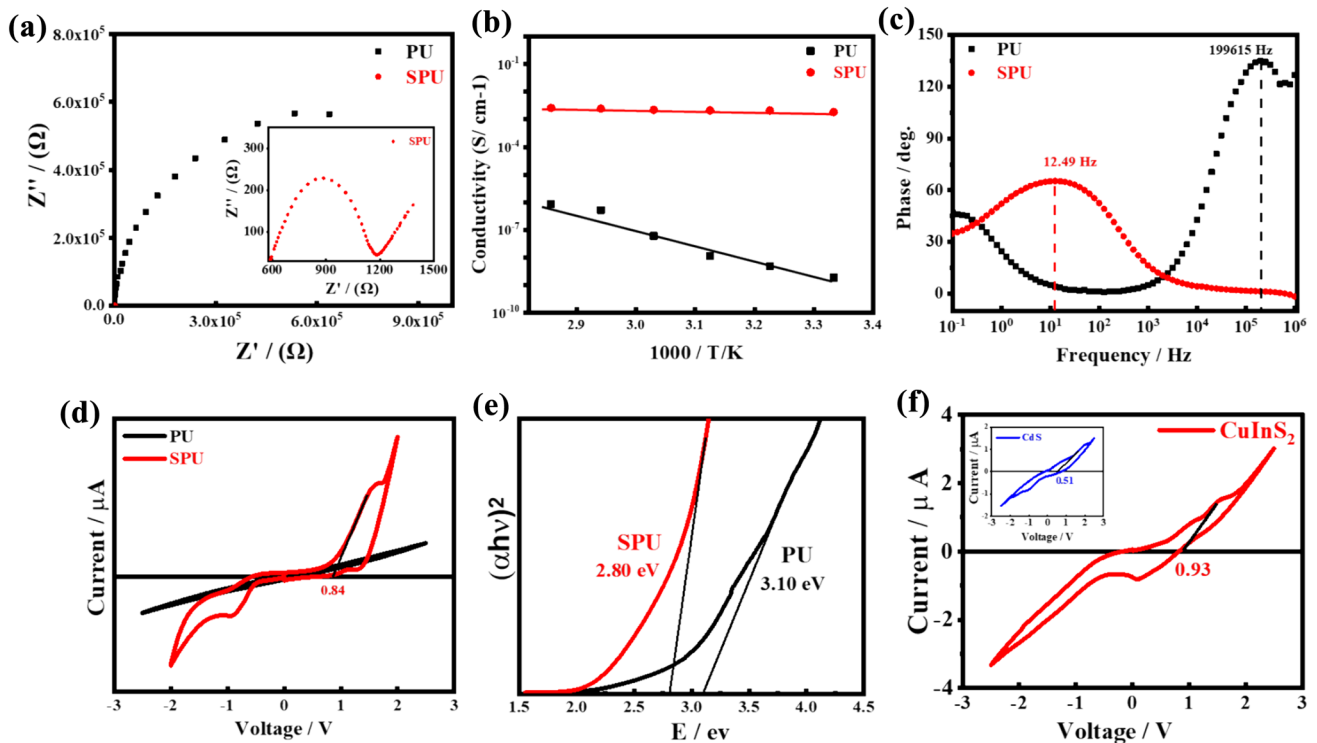


Fig. 3 **a** Electrochemical impedance spectroscopic measurements, Nyquist plots of the pure PU and SPU polymer; **b** Arrhenius plots of pure and functionalized PU (SPU); **c** Bode plots of QDSSCs based on the pure PU and SPU gel electrolytes; **d** cyclic voltammetry measure-

ments of pure (PU) and functionalized polymer (SPU); **e** optical band gap of the pure PU and functionalized PU; and **f** cyclic voltammetry measurements of CdS (inset figure) and CuInS₂ QDs

are found; one is associated with the reduction process, which results in a negative current, and the other is associated with the oxidation process, which produces a positive current. The onset of oxidation and reduction potential of the CV curves are used to calculate the HOMO and LUMO energy levels of the materials. The HOMO and LUMO energy levels of the materials play an important role which are directly affected by the transportation rate of electron and holes. The current voltage curve of PU and SPU are shown in Fig. 3d. The E_{OX} value is 0.84 V for SPU polymer and the E_{HOMO} is calculated to be of -5.24 eV from Eq. (3), while no oxidation and reduction peaks are found for pure PU in this current–voltage range. The optical band gap values, measured through UV–vis spectra, are found to be 3.10 and 2.80 eV for PU and SPU, respectively, using the Tauc's plots, shown in Fig. 3e. The E_{LUMO} value is determined by using the optical band gap in Eq. (4), and E_{HOMO} is obtained from CV measurement. Hence, E_{HOMO} and E_{LUMO} values for SPU is found to be -5.24 and -2.44 eV, respectively. Figure 3e displays the CV patterns of CdS (inset Figure) and CuInS₂ with E_{OX} values of 0.51 and 0.93 for CdS and CuInS₂, respectively. The observed E_{HOMO} values of CdS and CuInS₂ are -4.98

and -5.33 eV, respectively, whereas the estimated E_{LUMO} values are -2.73 and -3.48 eV.

Light Harvesting Efficiency and Electron–Hole Transfer Reaction

In order to construct effective photovoltaic devices, active materials with better light harvesting efficiency (LHE) and higher LHE value will produce more excitons when exposed to solar radiation. The Data shown in Fig. 4a illustrates the light harvesting efficiency (LHE) of TiO₂/CdS, TiO₂/CuInS₂, and TiO₂/CdS/CuInS₂ systems. The cosensitized TiO₂/CdS/CuInS₂ photoanode have greater LHE value than single loaded QDs such as TiO₂/CdS, and TiO₂/CuInS₂, which makes it suitable as active materials in the fabrication of photovoltaic devices. In order to create an energy profile diagram and identify appropriate matches, the E_{HOMO} and E_{LUMO} of prepared SPU polymer, and VB and CB of the synthesized QDs are combined with energy level of the Pt counter electrode. Figure 4b displays the energy profile diagram of the prepared polymer gel electrolyte (SPU), CdS, and CuInS₂ QDs with Pt counter electrode. It is clear from the energy profile diagram that the energy levels of HOMO of gel polymer electrolytes (-5.24 eV) is very close to VB of

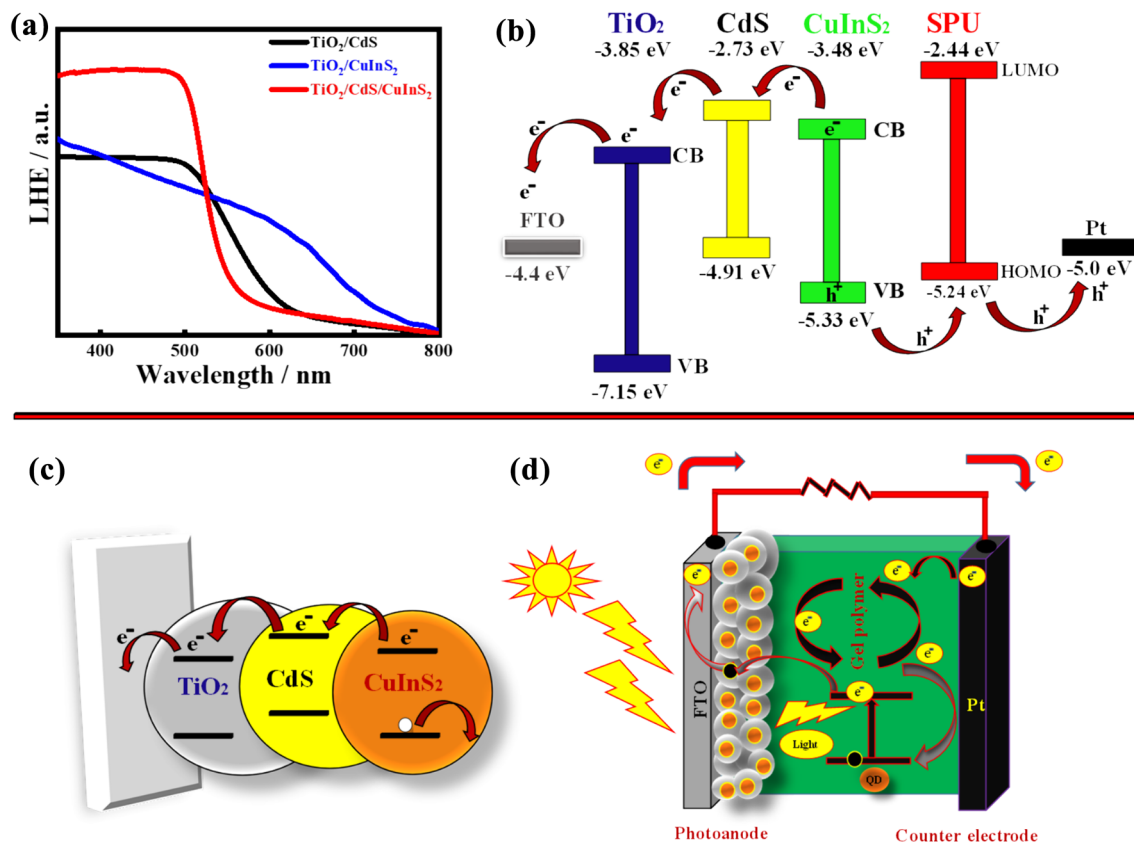


Fig. 4 **a** The light harvesting efficiency (LHE) of TiO₂/CdS, TiO₂/CuInS₂, and TiO₂/CdS/CuInS₂ photoanodes; **b** Energy level diagram of TiO₂, CdS, CuInS₂ with SPU polymer gel electrolyte; **c** schematic diagram of the layer-by-layer structure of TiO₂/CdS/CuInS₂ photoan-

ode showing the flow of electron and hole; and **d** the generation of electric current (electron hole transfer reaction) after the exposure of solar radiation in the fabricated QDSSCs devices

CuInS₂ (− 5.33 eV) (meagre difference of 0.09 eV), so that hole transportation becomes fast from VB of QDs (CuInS₂) to HOMO level of polymer gel electrolyte. This is to mention that VB of CdS (− 4.91 eV) is sufficiently differ from HOMO level of SPU (− 5.24 eV) which hinder the flow of holes from CdS to gel electrolyte. The addition of auxiliary CuInS₂ layer helps reducing the difference of energy level gap and thereby enhance the flow of holes from active materials to gel electrolyte or in other word the auxiliary CuInS₂ layer reduce the chance of recombination of electro-hole pair. Lower CB of CuInS₂ (− 3.48 eV) as compared to CdS (− 2.73 eV) further increases the gap between CB of CuInS₂ and LUMO of gel electrolyte. By this process, the chances of electron transport to gel electrolyte reduces significantly. The electron transfer rate is then faster from CB of CdS to TiO₂ so that CdS along with the cosensitizer (CuInS₂) plays an important role in the fabrication of devices. The prepared photoanode (TiO₂/CdS/CuInS₂) have fast hole transportation as well as higher electron transfer rate, hence, the cosensitized photoanode is beneficial for the fabrication of devices.

Figure 4c illustrates the schematic diagram of the layer-by-layer structure of TiO₂/CdS/CuInS₂ photoanode and the generation of electric current (electron hole transfer reaction) after the exposure of solar radiation which describe the extra electron (hot electron) excited from the cosensitizer. Complete fabricated devices are shown in Fig. 4d indicating the flow of electron and holes in bit excess. The constructed photoanode was exposed to solar radiation, CuInS₂ QDs along with CdS absorb the light and produced excitons (electron-hole pairs) and the excited electrons move from the conduction band (CB) of CuInS₂ to the TiO₂ through CdS energy levels and further transport to the external circuit, and the holes are moving from the VB of the CuInS₂ QDs directly to the HOMO energy levels of polymer gel electrolyte and then to the counter electrode to complete the circuit resulting produce an electric current.

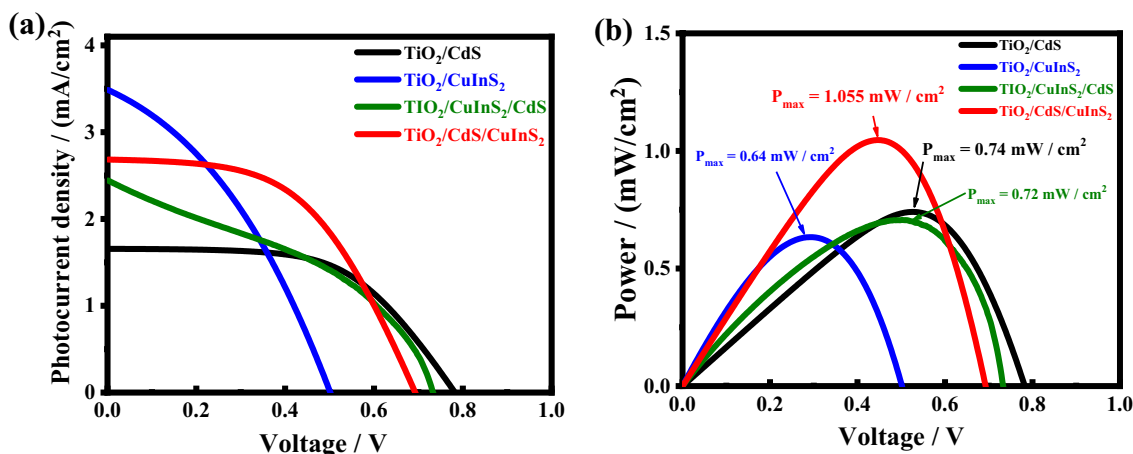


Fig. 5 **a** The photocurrent density and open-circuit voltage are computed using J-V characteristics curve under 1 sun irradiation; and **b** power conversion efficiency of the fabricated QDSSCs is computed using power voltage curves

Table 1 Photocurrent density, fill factor, open circuit voltage, and power conversion efficiency of different cells using the TiO₂/CdS, TiO₂/CuInS₂, and TiO₂/CdS/CuInS₂ photoanodes employing SPU polymer gel electrolyte

Photo anode	J_{sc} (mA/cm ²)	V_{oc} (volt)	Fill factor	Efficiency
TiO ₂ /CdS/CuInS ₂	2.70	0.68	0.58	1.05
TiO ₂ /CuInS ₂ /CdS	2.44	0.73	0.40	0.71
TiO ₂ /CuInS ₂	3.48	0.50	0.36	0.64
TiO ₂ /CdS	1.66	0.77	0.55	0.74

Photovoltaic Performance

Figure 5a shows the photocurrent–voltage (J-V) characteristics curve of the TiO₂/CdS/CuInS₂ photoanode with prepared polymer gel electrolyte (SPU) by employing the Pt counter electrode to fabricate the QDSSCs under the 1 sun solar irradiation with light intensity of 100 mWcm⁻².

The fabricated device with TiO₂/CuInS₂ photoanode, prepared polymer gel electrolyte and Pt as a counter electrode show the high photocurrent density J_{max} ~3.48 mA/cm² and 0.50 V open circuit voltage (V_{oc}) with low fill factor of 0.36 resulting lower power conversion efficiency (η) = 0.64%. Similarly, TiO₂/CdS photoanode with gel electrolyte exhibit low photocurrent density J_{max} ~1.66 mA/cm² and 0.77 V as open circuit voltage (V_{oc}) with the fill factor of 0.55 resulting poor power conversion efficiency (η) = 0.74%. In order to enhance the efficiency, cosensitized photoanode (TiO₂/CdS/CuInS₂) has been employed which demonstrates the photocurrent density J_{max} ~2.7 mA/cm² and open circuit voltage (V_{oc}) of 0.68 V with much improved fill factor of 0.58 resulting higher power conversion efficiency (η) = 1.05%. Figure 5b shows the power-voltage curve, which illustrate how the maximum

power varies with solar radiation. Table 1 represents, open circuit voltage, fill factor, photocurrent density, and power conversion efficiency for fabricated photovoltaic devices with different photoanodes. This is to mention that the relative layer structure (TiO₂/CuInS₂/CdS) of photoanode results in poor efficiency of (0.71%) mainly because of energy level position from which transport of electron and hole suffers a hindrance and recombination of electron–hole pair.

The cosensitized system's higher efficiency can be attributed to the complementary effect of CdS and CuInS₂ QDs on light harvesting, as previously discussed. Additionally, the stepwise band-edge level structure of CdS/CuInS₂ QDs facilitates the rate of electron ejection from CuInS₂ QDs and excited electron transports from CdS QDs to TiO₂. It is noteworthy that single photoanode, such as TiO₂/CuInS₂, exhibits a significantly low PCE (η) of 0.64% while cosensitized photoanode enhance the efficiency considerably. However, an optimum amount of CdS QDs layer deposition in between TiO₂ and CuInS₂ QDs demonstrate a significant effect in terms of power conversion efficiency. The fabricated device includes cosensitized photoanode TiO₂/CdS/CuInS₂, functionalized polymer gel electrolyte (SPU), and Pt as counter electrode and these fabricated devices show a better performance as compared to the single loaded QDs such as TiO₂/CdS and TiO₂/CuInS₂ photoanode.

Conclusion

Ionic sulfonate groups have been incorporated into thermoplastic polyurethane by successful chemical synthesis of polyurethane followed by functionalization. FTIR, UV–vis and ¹H-NMR spectroscopic techniques have been employed

to confirm the functionalization. PU ionomer is transformed into the appropriately conducting and hydrophilic media that may be used as gel electrolytes in solar cells applications. Adding CuInS₂ QDs as a cosensitizer has increased the power conversion efficiency of conventional CdS based sensitized solar cells. The cosensitized CdS/CuInS₂ photoelectrode has a complimentary impact on light harvesting, as shown by the UV–vis absorption spectra. CuInS₂ deposition has increased the sensitivity of CdS-sensitized TiO₂ photoanode. CuInS₂ considerably increase the photoconversion efficiency of the CdS/CuInS₂ cosensitized photoelectrodes, as seen from the J-V characteristics arising from better transport of electron and holes and thereby avoid the recombination process, as explained from the relative energy diagram. The TiO₂/CdS/CuInS₂ photoelectrode with SPU polymer gel electrolyte achieves the highest photoconversion efficiency of 1.05% under 1 sun illumination, which is approximately 42% higher than that of photoanodes without CuInS₂.

Data availability The data that support the findings of this study are available from the corresponding author upon reasonable request.

Declarations

Conflict of interest The authors declare no conflict of interest for this manuscript.

References


- Badawi A, Al-Hosiny N, Abdallah S, Negm S, Talaat H (2013) Tuning photocurrent response through size control of CdTe quantum dots sensitized solar cells. *Sol Energy* 88:137–143
- Bera D, Qian L, Tseng TK, Holloway PH (2010) Quantum dots and their multimodal applications: a review. *Mater* 3:2260–2345
- Boschloo G, Hagfeldt A (2009) Characteristics of the iodide/triiodide redox mediator in dye-sensitized solar cells. *Acc Chem Res* 42:1819–1826
- Climate Watch (2023) Historical emissions. <https://climatewatchdata.org/data-explorer/historical-emissions>. Accessed 23 Sept 2023
- Du J et al (2016) Zn-Cu-In-Se quantum dot solar cells with a certified power conversion efficiency of 11.6%. *J Am Chem Soc* 138:4201–4209
- Energy Institute (2023) Statistical review of world energy. <https://www.energyinst.org/statistical-review/home>. Accessed 23 Sept 2023
- Gao XF et al (2009) CdTe quantum dots-sensitized TiO₂ nanotube array photoelectrodes. *J Phys Chem C* 113:7531–7535
- Gerischer H, Luebke M (1986) A particle size effect in the sensitization of TiO₂ electrodes by a CdS deposit. *J Electroanal Chem Interfacial Electrochem* 204:225–227
- Green MA (2001) Third generation photovoltaics: ultra-high conversion efficiency at low cost. *Prog Photovolt Res Appl* 9:123–135
- Gu Y et al (2019) Preparation and photoelectric properties of cadmium sulfide quantum dots. *Chinese Phys B* 28:47803
- Jara DH, Yoon SJ, Stamplecoskie KG, Kamat PV (2014) Size-dependent photovoltaic performance of CuInS₂ quantum dot-sensitized solar cells. *Chem Mater* 26:7221–7228
- Kamat PV (2008) Quantum dot solar cells. Semiconductor nanocrystals as light harvesters. *J Phys Chem C* 112:18737–18753
- Kohtani S, Kudo A, Sakata T (1993) Spectral sensitization of a TiO₂ semiconductor electrode by CdS microcrystals and its photoelectrochemical properties. *Chem Phys Lett* 206:166–170
- Kongkanand A, Tvrđy K, Takechi K, Kuno M, Kamat PV (2008) Quantum dot solar cells. Tuning photoresponse through size and shape control of CdSe-TiO₂ architecture. *J Am Chem Soc* 130:4007–4015
- Lan GY et al (2009) A simple strategy for improving the energy conversion of multilayered CdTe quantum dot-sensitized solar cells. *J Mater Chem* 19:2349–2355
- Lee YL, Lo YS (2009) Highly efficient quantum-dot-sensitized solar cell based on co-sensitization of CdS/CdSe. *Adv Funct Mater* 19:604–609
- Lee HJ et al (2008) CdSe quantum dot-sensitized solar cells exceeding efficiency 1% at full-sun intensity. *J Phys Chem C* 112:11600–11608
- Leonat L, Sbarcea G, Branzoi IV (2013a) Cyclic voltammetry for energy levels estimation of organic materials. *UPB Sci Bull Ser B* 75(3):111–118
- Li B, Wang L, Kang B, Wang P, Qiu Y (2006) Review of recent progress in solid-state dye-sensitized solar cells. *Sol Energy Mater Sol Cells* 90:549–573
- Li TL, Lee YL, Teng H (2011) CuInS₂ quantum dots coated with CdS as high-performance sensitizers for TiO₂ electrodes in photoelectrochemical cells. *J Mater Chem* 21:5089–5098
- Li TL, Lee YL, Teng H (2012) High-performance quantum dot-sensitized solar cells based on sensitization with CuInS₂ quantum dots/CdS heterostructure. *Energy Environ Sci* 5:5315–5324
- Liu D, Kamat PV (1993) Photoelectrochemical behavior of thin CdSe and coupled TiO₂/CdSe semiconductor films. *J Phys Chem* 97:10769–10773
- Liu S, Zhang H, Qiao Y, Su X (2012) One-pot synthesis of ternary CuInS₂ quantum dots with near-infrared fluorescence in aqueous solution. *Rsc Adv* 2:819–825
- Luo J et al (2013) Highly efficient core-shell CuInS₂-Mn doped CdS quantum dot sensitized solar cells. *Chem Commun* 49:3881–3883
- Mitchell K, Eberspacher C, Ermer J and Pier D (1988) Proc. 20th IEEE photovoltaic specialists conf. In proc. 20th IEEE photovoltaic specialists conf 1384–1389
- Nozik AJ (2002) Quantum dot solar cells. *Phys E Low-Dimensional Syst Nanostruct* 14:115–120
- Nozik AJ (2021) Quantization effects in semiconductor nanostructures and singlet fission in molecular chromophores for photovoltaics and solar fuels. *Chem Phys Rev* 2:21305
- O'Regan B, Grätzel M (1991) A low-cost, high-efficiency solar cell based on dye-sensitized colloidal TiO₂ films. *Nature* 353:737–740
- Okada K, Matsui H, Kawashima T, Ezure T, Tanabe N (2004) 100 mm × 100 mm large-sized dye sensitized solar cells. *J Photochem Photobiol A Chem* 164:193–198
- Pan Z et al (2014) High-efficiency 'green' quantum dot solar cells. *J Am Chem Soc* 136:9203–9210
- Prakash R, Maiti P (2020) Functionalized thermoplastic polyurethane gel electrolytes for cosensitized TiO₂/CdS/CdSe photoanode solar cells with high efficiency. *Energy Fuels* 34:16847–16857
- Prakash R, Das S, Maiti P (2023) Non-toxic CuInS₂ quantum dot sensitized solar cell with functionalized thermoplast polyurethane gel electrolytes. *Polymer (guildf)* 269:125708
- Privalov T, Boschloo G, Hagfeldt A, Svensson PH, Klöö L (2009) A study of the interactions between I⁻/I₃⁻ redox mediators and organometallic sensitizing dyes in solar cells. *J Phys Chem C* 113:783–790
- Ritchie H, Roser M and Rosado P (2022) Renewable energy. *Our World Data*

- Robel I, Subramanian V, Kuno M, Kamat PV (2006) Quantum dot solar cells. Harvesting light energy with CdSe nanocrystals molecularly linked to mesoscopic TiO₂ films. *J Am Chem Soc* 128:2385–2393
- Ross RT, Nozik AJ (1982) Efficiency of hot-carrier solar energy converters. *J Appl Phys* 53:3813–3818
- Santra PK, Nair PV, George Thomas K, Kamat PV (2013) CuInS₂-sensitized quantum dot solar cell. Electrophoretic deposition, excited-state dynamics, and photovoltaic performance. *J Phys Chem Lett* 4:722–729
- Schmitt-Rink S, Miller DAB, Chemla DS (1987) Theory of the linear and nonlinear optical properties of semiconductor microcrystals. *Phys Rev B* 35:8113
- Shay JL and Jack H (1975) Ternary chalcopyrite semiconductors: growth, electronic properties, and applications. *International Series on Science of the Solid State*
- Shockley W, Queisser HJ (1961) Detailed balance limit of efficiency of p-n junction solar cells. *J Appl Phys* 32:510–519
- Song H, Rao H, Zhong X (2018) Recent advances in electrolytes for quantum dot-sensitized solar cells. *J Mater Chem A* 6:4895–4911
- Sudhagar P et al (2009) The performance of coupled (CdS:CdSe) quantum dot-sensitized TiO₂ nanofibrous solar cells. *Electrochem Commun* 11:2220–2224
- Tian J et al (2014) A highly efficient (> 6%) Cd_{1-x}Mn_xSe quantum dot sensitized solar cell. *J Mater Chem A* 2:19653–19659
- Uenishi S, Tohyama K, Ito K (1994) Photovoltaic characteristics of thin film CdS/CuInS₂ heterojunctions. *Sol Energy Mater Sol Cells* 35:231–237
- Vogel R, Pohl K, Weller H (1990) Sensitization of highly porous, polycrystalline TiO₂ electrodes by quantum sized CdS. *Chem Phys Lett* 174:241–246
- Wang W et al (2018) Cosensitized quantum dot solar cells with conversion efficiency over 12%. *Adv Mater* 30:1705746
- Wu J et al (2008) An all-solid-state dye-sensitized solar cell-based poly(N-alkyl-4-vinyl-pyridine iodide) electrolyte with efficiency of 5.64%. *J Am Chem Soc* 130:11568–11569
- Wu J et al (2015) Electrolytes in dye-sensitized solar cells. *Chem Rev* 115:2136–2173
- Wurfel U, Cuevas A, Wurfel P (2015) Charge carrier separation in solar cells. *IEEE J Photovolt* 5:461–469
- Xia C et al (2014) One-step synthesis of near-infrared emitting and size tunable CuInS₂ semiconductor nanocrystals by adjusting kinetic variables. *CrystEngComm* 16:7469–7477
- Yang J, Zhong X (2016) CdTe based quantum dot sensitized solar cells with efficiency exceeding 7% fabricated from quantum dots prepared in aqueous media. *J Mater Chem A* 4:16553–16561
- Yang W, Chen X, Liu L, Yang Q, Yang P (2016) Light-scattering photoanodes from double-layered mesoporous TiO₂ nanoparticles/SiO₂ nanospheres for dye-sensitized solar cells. *Electrochim Acta* 213:1–7

Publisher's Note Springer Nature remains neutral with regard to jurisdictional claims in published maps and institutional affiliations.

Springer Nature or its licensor (e.g. a society or other partner) holds exclusive rights to this article under a publishing agreement with the author(s) or other rightsholder(s); author self-archiving of the accepted manuscript version of this article is solely governed by the terms of such publishing agreement and applicable law.

Authors and Affiliations

Ravi Prakash¹ · Amita Santra¹ · Sparsh Yaduka¹ · Pralay Maiti¹ 

✉ Pralay Maiti
pmaiti.mst@itbhu.ac.in

¹ School of Materials Science and Technology, Indian Institute of Technology (BHU), Varanasi 221005, India